water

MDPI

Article

Calcium Carbonate Formation in Groundwater-Supplied Drinking Water Systems: Role of CO_2 Degassing Rate and Scaling Indices Applicability

Raghda Hamdi [1,*] and Mohamed Mouldi Tlili [2]

[1] Department of Chemistry, College of Science and Humanities in Al-Kharj, Prince Sattam bin Abdulaziz University, Al-Kharj 11942, Saudi Arabia
[2] Laboratory of Desalination and Natural Water Valorisation (LADVEN), Water Research and Technologies Center (CERTE), Techno-Park Borj Cedria, BP 273, Soliman 8020, Tunisia; mohamed.tlili@certe.rnrt.tn
* Correspondence: hamdi.raghda@gmail.com

Abstract: $CaCO_3$ precipitation is a ubiquitous and vital process with far-reaching implications for various natural systems. In drinking water supply networks, it creates malfunctions in the system, especially by pipes clogging. This is a common problem in Tunisia, particularly for systems supplied with groundwater. This work attempts to highlight the effect of dissolved CO_2 degassing kinetics and determine the most reliable scaling index to predict scaling. For this, a diagnosis of two drinking water circuits is followed by a laboratory study. Results of the field study show that the network scaling is controlled by the dissolved CO_2 content, which is significantly affected by the water/atmospheric air contact. The scale formed is mainly $CaCO_3$–calcite. A laboratory-scale simulation of the natural phenomenon using an experimental setup of the fast-controlled precipitation method (FCP) was performed. The result shows that a low CO_2 content is a necessary condition for a supersaturated system regarding calcite but not sufficient for precipitation to take place. The precipitation can occur at very low supersaturations if time is allowed for stable nuclei to form, explaining the scaling of drinking water networks. The fundamental and applied study of the scaling indices shows that the Ryznar stability index (RSI) is the most adaptable index for predicting scale formation.

Keywords: drinking water system; calcium carbonate precipitation; CO_2 degassing; scaling indices

check for updates

Citation: Hamdi, R.; Tlili, M.M. Calcium Carbonate Formation in Groundwater-Supplied Drinking Water Systems: Role of CO_2 Degassing Rate and Scaling Indices Applicability. *Water* **2024**, *16*, 2159. https://doi.org/10.3390/w16152159

Received: 20 June 2024
Revised: 24 July 2024
Accepted: 29 July 2024
Published: 31 July 2024

Copyright: © 2024 by the authors. Licensee MDPI, Basel, Switzerland. This article is an open access article distributed under the terms and conditions of the Creative Commons Attribution (CC BY) license (https://creativecommons.org/licenses/by/4.0/).

1. Introduction

Calcium carbonate precipitation is a fundamental geological and environmental process that occurs in various natural and industrial settings [1–3]. Throughout the precipitation process, a systematic transformation occurs in the initially precipitated phase, transitioning from a metastable state to a more stable, final crystalline phase. The formation of precipitation precursors in the supersaturated solution is imperative to alleviate this metastability. Numerous models have been proposed in the literature to elucidate the mechanism of $CaCO_3$ precipitation in an aqueous medium, highlighting the existence of these precursors [4–6]. Predominantly, these models posit that during the precipitation stage, the process initiates with the agglomeration of ions, forming a future precipitate in the shape of a cluster of $CaCO_3^\circ$ ion pairs or an association of hydrated Ca-CO_3, corresponding to one of the $CaCO_3$ hydrated phases [7]. The emergence of scaling phenomena in most natural water circuits stems from the formation of this precipitate, induced by the imbalance of the calco–carbonic system. Such imbalances may arise from the complex interaction of different chemical factors, such as heightened salt concentration in the environment, reduced CO_2 pressure due to degassing, increased temperature, and other contributing variables [8–10]. This scale formation creates malfunctions in the water systems: pipes clogging, reduction of water flow, corrosion under scale, damage to meters, etc.

In order to prevent the precipitation of calcium carbonate, it is crucial to understand the impact of each contributing factor. Among the common factors leading to $CaCO_3$ precipitation, the exchange of CO_2 between the solution and the atmosphere stands out as a frequent cause [11]. This exchange can result in elevated supersaturation levels, particularly concerning calcite, thereby triggering the precipitation process. Dissolved carbon dioxide, a ubiquitous component in aqueous solutions, exhibits a deep influence on the formation and stability of calcium carbonate minerals. As carbon dioxide dissolves in water, it undergoes chemical reactions, leading to the formation of carbonic acid. This acid can react with calcium ions, affecting the solubility of calcium carbonate and influencing the kinetics and thermodynamics of its precipitation. Understanding the dynamics of this interaction is crucial for unraveling the complexities of carbonate mineral formation and its consequences for geological processes and environmental conditions. Numerous studies highlight CO_2 degassing as a primary driver for natural water supersaturation, altering the system conditions favorably towards the nucleation of calcium carbonate crystals [12,13]. The absorption of CO_2 into an aqueous solution has the potential to induce either the formation or dissolution of $CaCO_3$ [14,15]. Conversely, CO_2 degassing leads to a rise in pH, initiating the formation of $CaCO_3$. Studies indicate that CO_2 outgassing results in significant scale formation, contributing to 60% to 90% of total calcite precipitation [16,17]. Therefore, it may be more efficient to focus on maintaining CO_2 in solution rather than attempting to prevent calcium carbonate nucleation. Cosmo et al. [18] confirmed that CO_2 has an important impact on the precipitation of $CaCO_3$ by enlarging the size of the aragonite crystals.

Thus, CO_2-degassing was used as a method to induce precipitation in numerous studies performed on $CaCO_3$ crystallization in aqueous media. The works were focused on the effects of several parameters, such as temperature, the presence of impurities, salts or scale inhibitors, etc., from the microstructural, thermodynamic, and kinetic points of view. Most of these studies were carried out on a laboratory scale. CO_2, as an important parameter in the $CaCO_3$ crystallization process and then the scaling phenomenon, has rarely been the subject of a proper study. Furthermore, having precise data on this parameter makes it possible to determine the water scaling power according to different scaling indices. These indices will be presented in detail and discussed in the following.

The present paper will then focus on the role of dissolved carbon dioxide on $CaCO_3$ crystallization, especially in drinking water networks. For that, this work will cover both an industrial-scale study and a laboratory study. It will start with a diagnosis of two drinking water networks. To understand and interpret the findings of the field study, laboratory experiments will be performed using an experimental device capable of simulating the scaling phenomenon in water networks. The combination of diagnosing real drinking water networks and subsequently validating findings through controlled experiments introduces a practical aspect that is often lacking in purely theoretical studies. Thermodynamic calculations coupled with kinetic studies of $CaCO_3$ precipitation under varying CO_2 content will be condcuted to provide a comprehensive understanding of the mechanisms involved.

2. Materials and Methods

For the field study, two drinking water supply networks, which will be detailed thereafter, are diagnosed. These networks are essential infrastructures responsible for delivering safe and clean water to the population. This study presents an assessment of two drinking water circuits in Tunisia, each experiencing significant scaling issues. These circuits are situated in separate regions within the northern part of the country. Spot water samples are collected from different components of the networks in containers made of glass to prevent contamination and preserve the integrity of the water samples. The pH and temperature are measured on-site using Hanna multi-parameters. The water samples are transported and preserved at 4 °C to maintain stability. Laboratory analysis is conducted within 48 h to analyze the concentrations of major ions essential for evaluating water quality: Ca^{2+},

Mg^{2+}, Na^{+}, HCO_3^{-}, Cl^{-}, and SO_4^{2-}. The colorimetric and titrimetric methods are used to determine and measure the concentration of these major ions.

The deposit scale was collected from the clogged pipes and analyzed using the X-ray diffraction (XRD) method with a diffractometer Philips X'PERT PRO (PANalytical, Philips, Amsterdam, The Netherlands) in step-scanning mode using Cu K (1.54 Å) radiation. The XRD patterns were chronicled in the angular range 2θ = 20–60, with a slight step size of 2θ = 0.017 and a fixed count time of 4 s. The software 'X-Pert HighScore Plus' was used to determine the XRD reflection positions. The XRD patterns of the formed precipitates were compared to those of the joint committee on powder diffraction standards.

For the laboratory study, precipitation tests of calcium carbonate were performed for various experimental conditions using the controlled precipitation method (FCP). The tested solution was pure calco–carbonic water (PCCW), prepared by dissolving a predefined amount of calcium carbonate (analytical grade, purity > 99%) in 1 L of distilled water under CO_2 bubbling as follows:

$$CaCO_3 + CO_2 + H_2O \rightarrow Ca^{2+} + 2HCO_3^{-} \quad (1)$$

The FCP method setup is presented in Figure 1. The temperature was controlled using a thermostatic water bath. The reactor is a polytetrafluoroethylene (PTFE) cell filled with 1 L of PCCW. To facilitate CO_2 degassing, the air–water contact surface is renewed by water stirring using a magnetic stirrer. The pH and resistivity values of the solution were regularly measured using a HI 110 pH meter (Hanna Instruments, Woonsocket, RI, USA) and a CDM 210 conductivity meter (Meter Lab, Radiometer Analytical's, Villeurbanne, France). The precipitation was monitored by EDTA complexometric titration of the calcium ion.

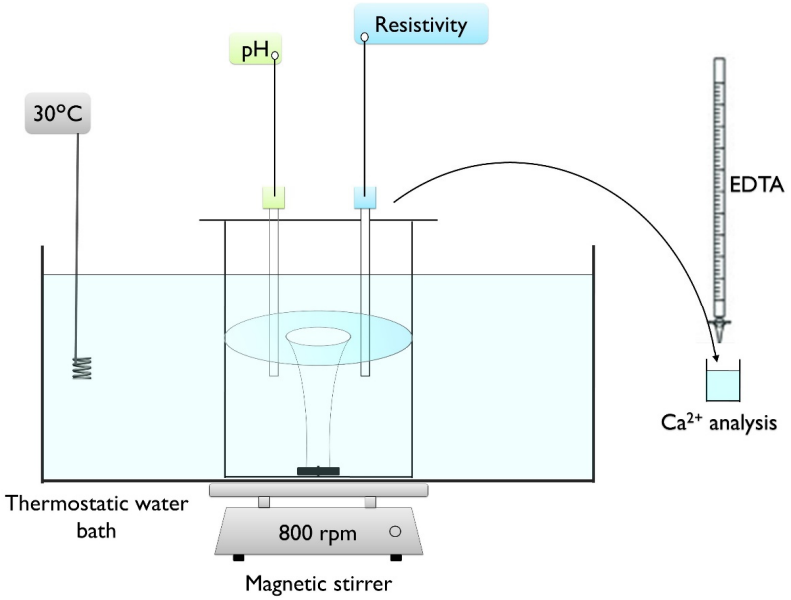


Figure 1. Fast-controlled precipitation method.

Figure 2 illustrates the curves of pH and resistivity for a typical FCP test using a 400 mg/L PCCW. The figure underlines the limit between the nucleation and growth of $CaCO_3$. Before the precipitation time "t_{prec}", the pH value increases with a slight resistivity variation. Resistivity variation is attributed to nuclei formation by ion pair agglomeration [7]. At the precipitation threshold corresponding to "pH_{prec}", the pH decreases, and the slope of the temporal evolution of resistivity deviates considerably. It consists of the $CaCO_3$-growth phase, which follows:

$$Ca^{2+} + HCO_3^{-} \rightarrow CaCO_3 + H^{+} \quad (2)$$

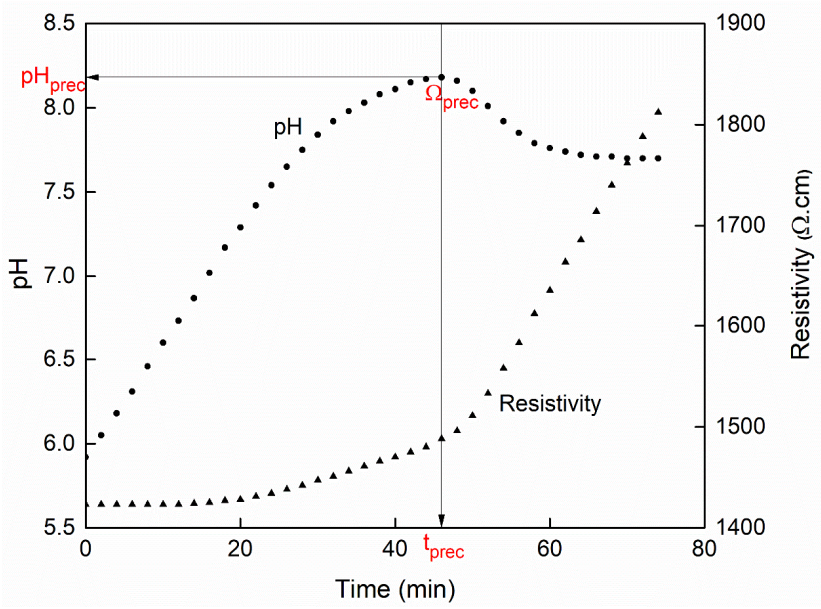


Figure 2. Temporal evolution of the pH and resistivity curves of a PCCW at 400 mg/L at 800 rpm.

3. Theoretical Calculations for Thermodynamic Analysis

3.1. Supersaturation Coefficient

Since the thermodynamic driving force of the precipitation process is supersaturation, the supersaturation coefficient (Ω) is considered to characterize the scaling potential of the water. The water is at equilibrium regarding the calco–carbonic system $CaCO_3$–CO_2–H_2O for Ω = 1. It is undersaturated and aggressive with respect to calcium carbonate if Ω < 1 and supersaturated, and, theoretically, $CaCO_3$ nucleation could spontaneously occur for Ω > 1. Knowing the water temperature, pH, and chemical composition, Ω is calculated according to

$$\Omega_{CaCO_3} = \frac{\left[Ca^{2+}\right]\cdot\left[CO_3^{2-}\right]\cdot\gamma_{Ca^{2+}}\cdot\gamma_{CO_3^{2-}}}{K_s(calcite)} \quad (3)$$

where [i] is the concentration of *i*th ion and γ_i is the ion activity coefficient calculated using Davies [19] equation:

$$log(\gamma_i) = -Az_i^2\left(\frac{\sqrt{I}}{1+\sqrt{I}} - 0.3I\right) \quad (4)$$

where $A = 1.82 \times 10^6(\varepsilon T)^{-3/2}$, T is the temperature in Kelvin and ε is the water dielectric constant calculated according to Malmberg and Maryott's [20] equation:

$$\varepsilon = 87.74 - 0.40008\cdot T + 0.0009398\cdot T^2 - 0.000001411\cdot T^3 \quad (5)$$

and I is the ionic strength calculated as follows:

$$I = \frac{1}{2}\sum_{i=1}^{n} c_i z_i^2 \quad (6)$$

where c_i and z_i are the concentration and the charge of the *i*th ion, respectively.

The solubility product of calcite, the most stable form of calcium carbonate $K_{s/calcite}$, is calculated using the Plummer and Busenberg [21] equation:

$$logK_{s/calcite} = -171.9065 - 0.077993T + \frac{2839.319}{T} + 71.595logT \quad (7)$$

where T is the temperature in Kelvin.

3.2. Scaling Indices

From the beginning of the 20th century, researchers were interested in developing indices allowing the determination of the $CaCO_3$ scale formation threshold and the water scaling potential according to its chemical composition and the conditions of its use. Among these indices, the most well-known are the Langelier saturation index (LSI) [22] and the Ryznar stability index (RSI) [23], expressed by Equations (8) and (9).

$$LSI = pH - pH_s \tag{8}$$

$$RSI = 2pH_s - pH \tag{9}$$

For both indices, pH represents the solution's effective pH, and pH_s is the pH at which any water with a given calcium content and alkalinity is in equilibrium (neither oversaturated nor undersaturated in calcium carbonate).

In the equation of the Langelier index, the pH_s is determined from Equation (10), the simplest form applicable to the natural water within the pH range of 7 to 9.5.

$$pH_S = pK_2' - pK_{s/calcite}' + p\left(Ca^{2+}\right) + p(alk) \tag{10}$$

where $p(Ca^{2+})$ and p(alk) are the negative logarithms of the molal and equivalent concentrations of calcium and titratable base, respectively. K_2' and K_s' are apparent constants computed from the true thermodynamic constants K_2 and K_S: the second dissociation constant for carbonic acid and the activity product of $CaCO_3$–calcite, respectively. The water is scale-forming for positive LSI. If not, water is in a calco–carbonic equilibrium state (LSI = 0) or undersaturated (LSI < 0).

For Ryznar, the Langelier Index is only qualitative and does not indicate how much calcium carbonate will deposit or whether a state of supersaturation will be present, which will be great enough to produce a precipitate. Thus, the empirical stability index proposed by Ryznar (Equation (9)) is not only an index of $CaCO_3$ saturation but is also of quantitative significance; the amount of calcium carbonate that will be formed can be estimated. In the RSI (Equation (9)), Ryznar used for the pH_s the equation of Larson and Buswell [24] (Equation (11)).

$$pH_S = pK_2 - pK_S + p\left(Ca^{2+}\right) + p(alk) + 9.3 + \frac{2.5\sqrt{I}}{1 + 5.3\sqrt{I} + 5.5I} \tag{11}$$

In this equation, (Ca^{2+}) and *(alk)* are expressed in parts per million as Ca and $CaCO_3$, respectively. K_2 and K_s are the true thermodynamic constants of the second dissociation of carbonic acid and the activity product of $CaCO_3$, respectively. I is the ionic strength of the water.

Water having a stability index of approximately 6 or less is definitely scale-forming, while an RSI above 6.5 may not give a protective coating of $CaCO_3$ scale, and the water tends to be corrosive. For an RSI in between, water is in equilibrium with respect to scale and metal.

Later, from their work on the thermodynamics of the calco–carbonic system, researchers have shown the occurrence of a large supersaturated domain with respect to calcite called the metastable domain, where the precipitation does not occur spontaneously. For Gal et al. [25], the precipitation of any one of the hydrated forms ($CaCO_3{\cdot}H_2O$, $CaCO_3{\cdot}6H_2O$, and ACC: amorphous $CaCO_3$) could be responsible for the breakdown of the metastable state. Likewise, Elfil and Roques [26] have shown that water keeps a metastable pH ranging from the saturation pH regarding the calcite form to that of the monohydrate form $CaCO_3{\cdot}H_2O$. The solubility product of $CaCO_3{\cdot}H_2O$ constitutes the lower limit for spontaneous calcium carbonate nucleation. This finding led Elfil and Hannachi [27] to propose a new saturation index called MLSI (Equation (12))/Monohydrated form of

the Langelier saturation index. The water is scale-forming for positive MLSI, whereas spontaneous precipitation cannot occur for negative MLSI values.

$$MLSI = pH - pH_{s/MCC} \tag{12}$$

where pH represents the solution's effective pH, while $pH_{S/MCC}$ denotes the saturation pH regarding the monohydrate calcium carbonate (MCC):

$$pH_{S/MCC} = pK_2 - pK_{S/MCC} - log\gamma_{HCO_3^-} - log\gamma_{Ca^{2+}} - log\left[Ca^{2+}\right] - log[alk] \tag{13}$$

where $\left[Ca^{2+}\right]$ and $[alk]$ are the molar concentrations of calcium and bicarbonate ions. Plummer and Busenberg [21] constants were used for K_2 and $K_{s/MCC}$ calculation. γ_i is the ion activity coefficient.

3.3. Discussion on the Prediction of the Water-Scaling Power Using Different Indices

In Figure 3, we have tried to illustrate the different scaling indices LSI, RSI, and MLSI on the same graph to show the differences in predicting whether water is scale-forming or not for concentrations of dissolved $CaCO_3$ ranging from 100 to 400 mg/L. To do it, the supersaturation coefficient Ω is calculated at 20 °C using Equation (3) at pH_s for LSI (LSI = 0) and MLSI (MLSI = 0) and at pH = $2pH_s$—RSI for RSI of 6 and 6.5. pH_s was calculated for different pure calco–carbonic solutions using Equation (14) for LSI and RSI and Equation (13) for MLSI.

$$pH_S = pK_2 - pK_{S/calcite} - log\gamma_{HCO_3^-} - log\gamma_{Ca^{2+}} - log\left[Ca^{2+}\right] - log\left[HCO_3^-\right] \tag{14}$$

where the constants K_s and K_2 of Plummer and Busenberg [21] have used more recent data for their evaluation, and their variation with temperature and total dissolved salts are used.

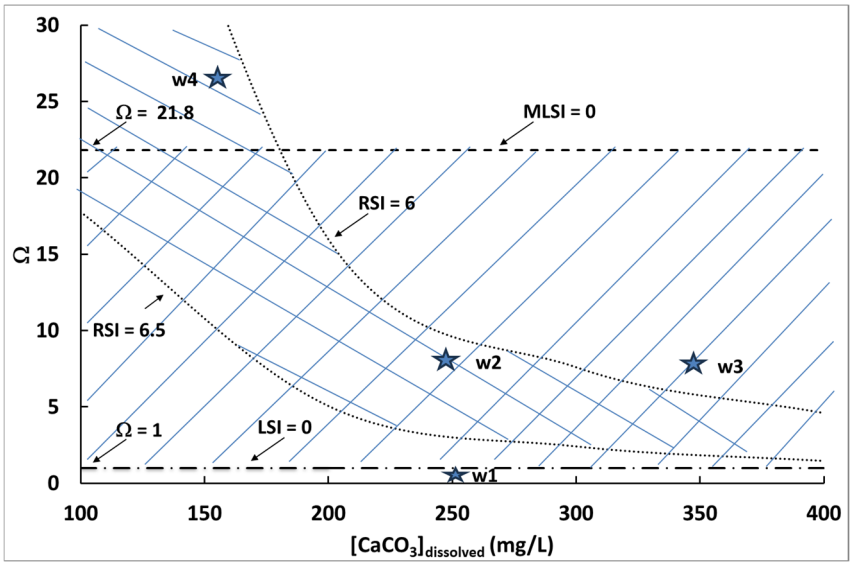


Figure 3. Equilibrium curves were calculated from LSI, RSI, and MLSI scaling indices in terms of supersaturation coefficient for different calco–carbonic water concentrations.

The curves in this figure delimit the zone where water is scale-forming from the one for which the water is undersaturated or in a metastable state. Considering the LSI, the water is scale-forming for Ω > 1 and undersaturated for Ω < 1. For MLSI, it is scaling if Ω > 21.8, in a metastable state for 1 < Ω < 21.8, and undersaturated for Ω < 1 regardless of the dissolved $CaCO_3$ concentration. Unlike MLSI, the equilibrium (metastable) domain determined by RSI is $CaCO_3$ concentration-dependent.

From this figure, it can be shown that if $\Omega < 1$ (e.g., w1-250 mg/L in Figure 3), the water is non-scale-forming for all indices. For $\Omega > 1$, this same water (w2-250 mg/L where $\Omega = 8$) is scale-forming regarding the LSI; however, it cannot spontaneously precipitate calcium carbonate considering MLSI and RSI. For the same supersaturation coefficient $\Omega = 8$, water more concentrated in $CaCO_3$ (w3-350 mg/L) remains in a metastable state for MLSI; however, it becomes scaling for RSI. This means that the Ryznar saturation index does not only consider the saturation state of the water but also its concentration in $CaCO_3$. Unlike high concentrations, water at low $CaCO_3$ concentrations, and high supersaturation (e.g., w4-150 mg/L; $\Omega = 28$), the MLSI predicts that water is scale-forming, while the RSI no.

Despite the differences recorded in predicting whether water is scale-forming or not, scaling indices remain an important tool in assessing the scale-formation risk for water operators in different sectors. The observed differences can be attributed to the methods used for $CaCO_3$ precipitation, which can notably affect the nucleation kinetics.

4. Results and Discussion

4.1. Scale Prediction in Drinking Water Systems: Case Study

The scaling phenomenon is widespread in the drinking water systems supplied with underground water in both northern and southern Tunisia. The clogging of the distribution pipes leads to serious hydraulic, social, and economic consequences: reduction in pressure, interruption of water supply, high maintenance costs, etc. Extensive research conducted on this subject indicates that, regardless of the physicochemical properties of the water, scaling issues manifest within a timeframe of 3 to 36 months, and the deposited mineral is mainly anhydrous calcium carbonate ($CaCO_3$) [28]. In the south of Tunisia, the exploitation of fossil water, which emerges at high temperatures (>60 °C), leads to the crystallization of $CaCO_3$ in its aragonite form [29,30]. However, apart from these hot waters, the calcite polymorph of calcium carbonate is the main sparingly soluble salt meted in the components of the water supply systems. This scale formation was attributed to the displacement of the calco–carbonic equilibrium towards $CaCO_3$ precipitation because of the CO_2 exchange between the underground water and the air poor in this gas in the cooling towers, reservoirs, and basins for pressure reduction (BPR) following the overall reaction presented by the equation:

$$Ca^{2+} + 2HCO_3^- \rightarrow CaCO_3 + CO_2 + H_2O \quad (15)$$

In what follows, the diagnosis of two drinking water circuits that encountered a serious scaling problem is presented. These circuits, located in distinct regions in the northern part of Tunisia, are schematically illustrated in Figure 4.

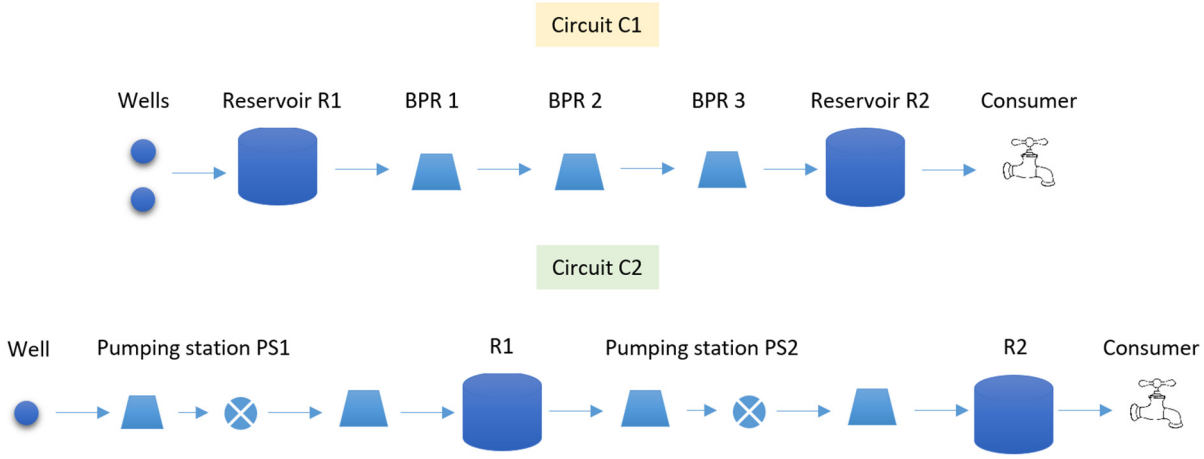


Figure 4. Simplified scheme of the drinking water supply Circuits C1 and C2.

Circuit 1 (C1) is supplied by the water from two wells initially collected in the reservoir R1. The physicochemical properties of the water in R1 sampled in the month of April for C1 and the water at the outlet of the well for C2 sampled in June are presented in Table 1.

Table 1. Physicochemical properties of the feed water for Circuits 1 and 2.

	θ °C	pH	TDS mg·L^{-1}	Ca^{2+} mg·L^{-1}	Mg^{2+} mg·L^{-1}	Na^{+} mg·L^{-1}	HCO_3^{-} mg·L^{-1}	SO_4^{2-} mg·L^{-1}	Cl^{-} mg·L^{-1}	K^{+} mg·L^{-1}
Circuit 1	20	7.48	698	106	46	87	239	144	177	-
Circuit 2	24	6.90	701	166	20	62	452	93	136	2

Table 1 shows that the salinity of these two waters (TDS at 105 °C) is close to 700 mg/L. However, the mass percent of calcium and bicarbonate, the main ions responsible for the $CaCO_3$ scale formation, are 49 and 88% in the waters of C1 and C2, respectively. Regarding the chemical properties of water, calcium carbonate is a sparingly insoluble salt that can precipitate. From a thermodynamic point of view, it crystallizes when the water is saturated with respect to the most stable phase calcite ($\Omega > 1$) and, subsequently, the pH exceeds the equilibrium pH_s (saturation pH calculated using Equation (13) for corresponding temperature): pH_s = 7.20 for C1 and 6.66 for C2.

As indicated in Table 1, upon circuit supply, the calco–carbonic system becomes unbalanced, with pH values of 7.48 for C1 and 6.90 for C2, slightly exceeding the pH_s, resulting in a tendency for the circuits to become clogged. However, the scaling of the pipes and reservoirs only becomes significant towards the far end of the network.

The X-ray diffraction analysis of the solids recuperated from the concrete and polyethylene pipes of C1 and C2, respectively (Figure 5), proves that the scale is mainly $CaCO_3$ calcite.

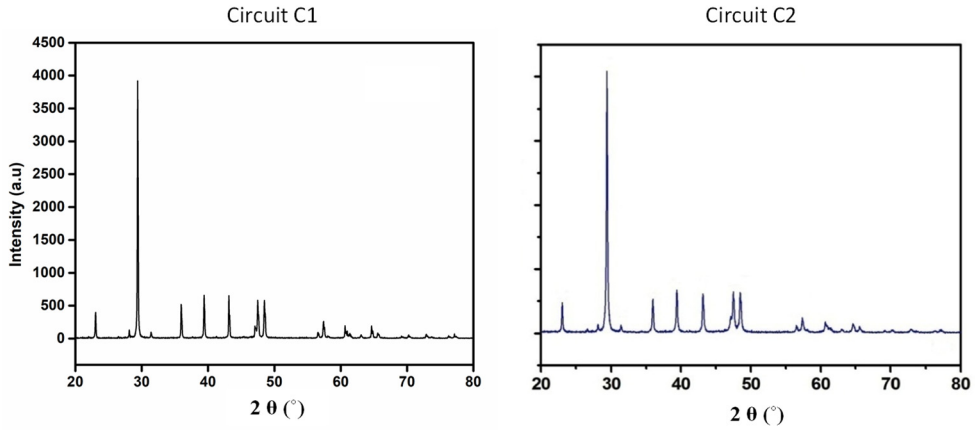


Figure 5. X-ray diffractograms of the scale recuperated from C1 and C2.

As shown in Table 2, the measured pH throughout the networks increases to reach a maximum of 8.30 at BPR2 and 7.78 at PS2 for C1 and C2, respectively. This can be attributed to the release of dissolved CO_2 when water encounters air. In the last portion of the circuits (from BPR2 for C1 and PS2 for C2), corresponding to the fouled pipes, there is a decrease in pH. This shows that the $CaCO_3$ scale is formed on the walls of different network components in contact with water. Indeed, the growth of $CaCO_3$ can be easily made by calcium and bicarbonate ions in supersaturated water, as follows:

$$Ca^{2+} + HCO_3^{-} \rightarrow CaCO_3 + H^{+} \quad (16)$$

Table 2. Evolution of the pH and the supersaturation coefficient in the diagnosed circuits.

Circuit 1	**R1**	**BPR1**	**BPR2**	**BPR3**	**R2**	**Consumer**
pH	7.48	8.15	8.30	8.23	8.12	7.8
Ω	1.93	9.0	12.7	10.8	8.4	4.0
LSI	0.28	0.95	1.10	1.03	0.92	0.6
RSI	6.92	6.25	6.10	6.17	6.28	6.60
MLSI	−1.05	−0.38	−0.23	−0.30	−0.41	−0.73
Circuit 2	**Well**	**PS1**	**R1**	**PS2**	**R2**	**Consumer**
pH	6.95	7.1	7.52	7.78	7.6	7.45
Ω	1.68	2.75	7.22	13.14	8.68	6.15
LSI	0.29	0.44	0.86	1.12	0.94	0.79
RSI	6.37	6.22	5.80	5.54	5.72	5.87
MLSI	−1.05	−0.90	−0.48	−0.22	−0.40	−0.55

To understand the appearance of the scaling phenomenon in such real circuits and to know about the applicability and reliability of the different scaling indices in predicting the scaling risk of drinking water networks in Tunisia, scaling indices were calculated throughout C1 and C2. Since temperature is an important parameter in the process of $CaCO_3$ precipitation, Table 2 presents the supersaturation coefficient and saturation indices values calculated at the real temperature of 20 °C for C1 and 24 °C for C2.

Positive LSI values were recorded from the beginning of both circuits, meaning that water is scale-forming, according to Langelier. Nevertheless, the precipitation occurs only for LSI~1.1 for both circuits, corresponding to a supersaturation coefficient Ω~13. This suggests that LSI cannot predict scale formation accurately and confirms the existence of a metastable state where spontaneous precipitation cannot occur, which agrees with several works conducted at laboratory scale [7,26]. Unlike the Langelier index, which predicts the scaling of the entire circuit, the calculated MLSI values are negative, and no precipitation is possible throughout the circuit, which is not the case.

The calculated Ryznar saturation index (RSI) for C1 shows that water is aggressive regarding the metal and calcium carbonate at the beginning of the circuit (RSI > 6.5) and in the metastable state in the rest of the circuit (6 < RSI < 6.5). At pH 8.30 (BPR2), where the scale starts to form, the RSI is 6.10, very close to the lower limit of the equilibrium domain defined by Ryznar (RSI = 6). Considering errors in pH and temperature measurement and chemical analyses, the true RSI value may be close to or lower than 6. On the other hand, it is possible that the scale was formed when the ambient temperature was higher (in the summer). Indeed, water temperature varies depending on the season from 10 to 30 °C; e.g., the calculated RSI is 5.90 for a water temperature of 25 °C and 5.76 for a temperature of 30 °C. For C2, RSI perfectly predicts the real situation. At PS2, where the pH is the highest (RSI = 5.54), the water is scale-forming.

From the above, it can be concluded that natural water intended for drinking can maintain a metastable state where spontaneous precipitation does not occur. This suggests that the Langelier saturation index is not adequate for determining the scaling power of water. The metastable domain extends from the equilibrium with respect to calcite until the equilibrium of one of the hydrated forms of calcium carbonate is exceeded, which will serve as a precursor to precipitation [31]. El fil et al. [26,27] defined the upper limit of this metastable equilibrium state as the monohydrate $CaCO_3 \cdot H_2O$ equilibrium. In a previous study [6], we have shown that $CaCO_3$ can precipitate in this metastable domain.

In light of the results presented above, which show that precipitation can take place without reaching equilibrium with respect to these hydrated forms (MLSI < 0), we propose in what follows to focus on the nucleation kinetics by varying the CO_2 degassing rate in order to explain the disparity recorded in determining the water scaling power using different scaling indices.

4.2. Effect of CO_2 Degassing Rate on $CaCO_3$ Nucleation Kinetics and Precipitation Threshold

4.2.1. Effect of the Stirring Rate

Precipitation tests were performed using the FCP method in a 400 mg/L $CaCO_3$-PCCW at 30 °C at 2 rotation rates of the magnetic bar of 400 and 800 rpm. This $CaCO_3$ concentration is close to that of the circuit C2 water. Figure 6 presents the experimental measurements of $\Delta_{Resistivity}$ versus pH from the beginning of the experiment (t = 0) to t = t_{prec} (nucleation period).

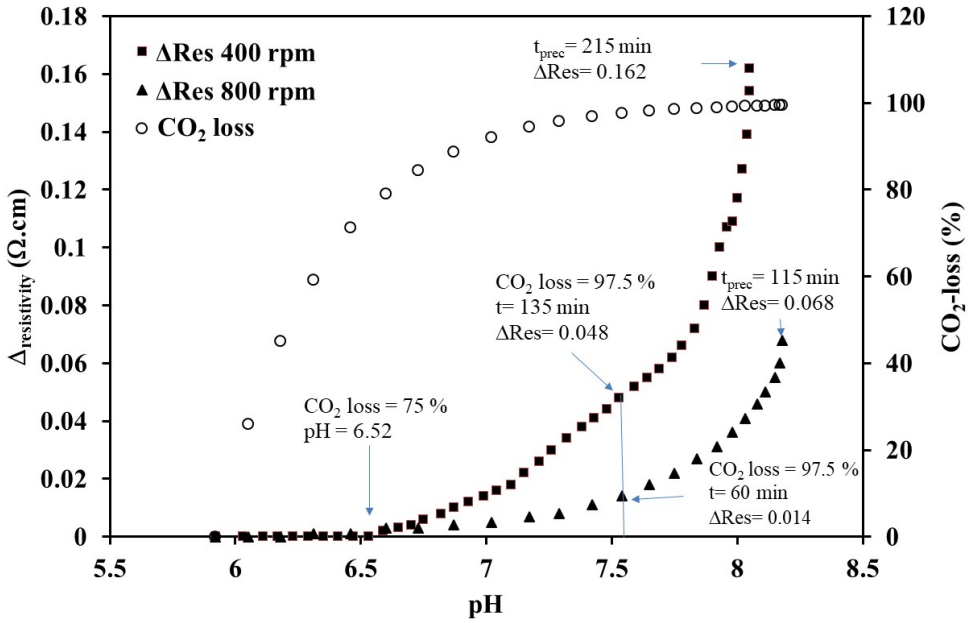


Figure 6. $\Delta_{Resistivity}$ vs. pH curves at the $CaCO_3$-nucleation period for 400 and 800 rpm.

Figure 6 shows that the water resistivity variation is appreciable only at pH 6.52, close to the pH_{eq} regarding calcite, where 75%, with respect to the initial content, of CO_2 is lost. The resistivity variation was attributed, in a previous study [7], to the ion pairs $CaCO_3^\circ$ formation, which plays the role of precursor for calcium carbonate nucleation. These ion pairs are crucial in the early stages of calcium carbonate formation, facilitating the subsequent growth of crystals and precipitation. For the same pH of 7.53, in the nucleation step, the loss of CO_2 was about 97% after 135 min with an agitation of 400 rpm and only after 60 min for 800 rpm. This finding underscores the influence of agitation speed on the kinetics of CO_2 degassing and subsequent nucleation processes. At this saturation state (Ω = 11), the variation in solution resistivity is more important when the CO_2 degassing is slower. $\Delta_{Resistivity}$ values are three times greater at 400 rpm than at 800 rpm. Consequently, the parameter time is crucial in the nucleation process once the solution is supersaturated; nucleation can occur at lower supersaturation coefficients if sufficient time is allowed for the stable nuclei to form. The precipitation occurs for a longer precipitation time, t = 215 min for the experiment at 400 rpm, compared to 115 min for the run at 800 rpm, but at a lower pH and supersaturation coefficient of about 48 and 35, respectively.

Among the consequences of slow degassing compared to rapid degassing is reaching similar saturation states at longer times. The time factor seems to play not only an important role in the formation of clusters of ions in solution but also in the adhesion of scale on the walls. The longer time allows for the gradual formation and stabilization of these clusters, which serve as nuclei for calcium carbonate precipitation. Moreover, time affects the adhesion of scale to surfaces within the water distribution system. This is crucial because the formation and growth of scale on pipe walls can lead to operational inefficiencies and maintenance challenges. The percentage of heterogeneous precipitation $\%_{hete}$ is calculated using the weight method [32]. It decreases from 81 to 45% when the degassing rate is

slowed down. This can be attributed to the size of the formed nuclei, which is saturation state-dependent. Indeed, it has been demonstrated that when $CaCO_3$ clusters exceed a size of 10 nm, their adhesion to walls becomes difficult. When the degassing rate is rapid, these associations tend to rapidly enlarge in the solution due to the high supersaturation coefficient before reaching the cell walls. This phenomenon could account for scaling in real drinking water distribution circuits, even when the supersaturation coefficient does not surpass 20 but persists over extended periods, on the order of years.

4.2.2. Effect of the Saturation State on Precipitation Threshold Time

To better highlight the role of the time factor, besides the role of the thermodynamic state regarding the calco–carbonic system, in the $CaCO_3$ precipitation process, FCP tests were performed for different supersaturation coefficients. Constant Ω was obtained by stopping the exchange of dissolved CO_2 with air. This was conducted by closing the cell a few minutes before reaching the desired point. This keeps a balance between the CO_2 in the air in the closed reactor (the empty part) just below the solution and the dissolved CO_2.

Figure 7 illustrates the temporal evolution of pH in correlation with the equilibrium pH of various $CaCO_3$ varieties (represented by dotted lines) based on the stabilization pH (pH_{stab}). From a kinetic point of view, the time necessary to reach the precipitation threshold is higher as the pH is maintained at lower values. Indeed, according to Table 3, t_{prec} increases from 46 min for the open cell, where pH_{prec} = 8.18 and Ω_{prec} = 48, to 295 min for the closed cell, whose pH of stabilization value noted is pH_{stab}, which is equal to 7.45 and Ω_{prec} = 9. This observation underscores the critical role of pH in precipitation kinetics. The precipitation kinetics play a crucial role in defining the extent of the metastable domain in the solution. A longer stabilization time allows precipitation to initiate at lower pH values. Consequently, this occurs at lower supersaturation coefficients (Ω), indicating a more stable state of the solution with respect to calcium carbonate precipitation.

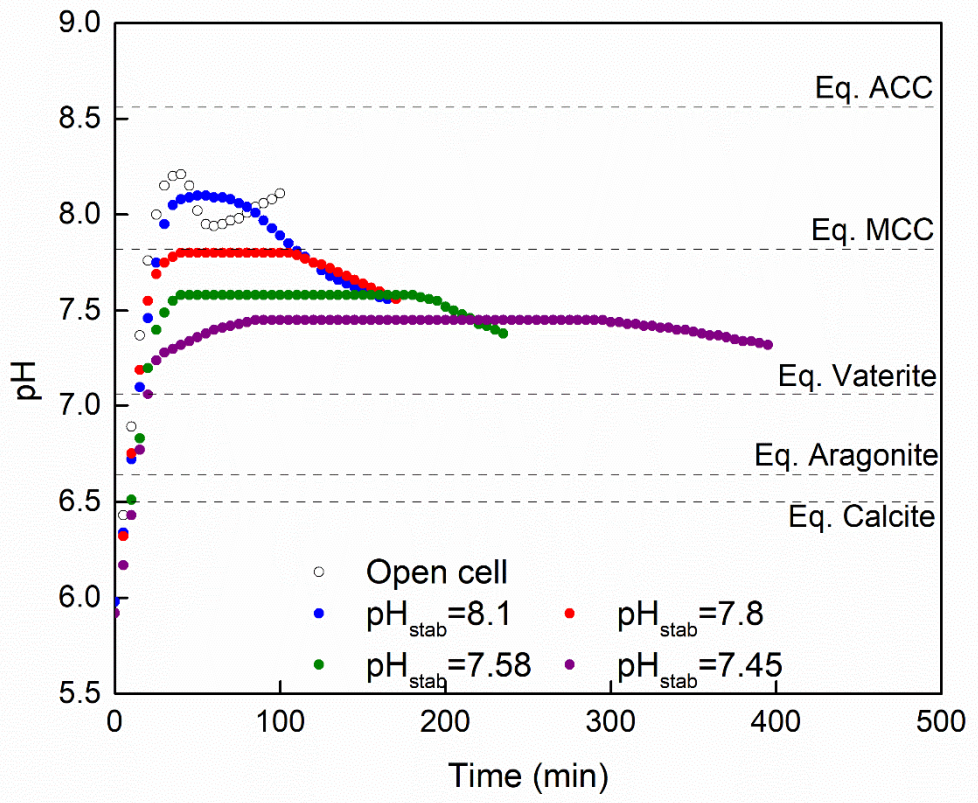


Figure 7. Temporal evolution of pH in correlation with the equilibrium pH of different CaCO3 varieties as a function of pH_{stab}.

Table 3. t_{prec}, Ω_{prec}, and scaling saturation indices (LSI, RSI, and MLSI) as a function of pH_{stab}.

pH_{stab}	t_{prec} (min)	Ω_{prec}	LSI	RSI	MLSI
8.18 (open cell)	46	48	1.66	3.78	0.34
8.10	55	40	1.58	3.86	0.26
7.80	105	20	1.28	4.16	−0.03
7.58	180	12	1.06	4.38	−0.25
7.45	295	9	0.93	4.51	−0.38
7.17	-	4.7	0.64	5.87	−0.35

As seen in Figure 7, precipitation is possible without reaching the equilibrium pH of the monohydrate calcium carbonate (MCC) for two experiments corresponding to pH_{stab} = 7.58 and 7.45. This outcome is surprising, as the majority of studies [27,33] concur that precipitation below the equilibrium pH of MCC is considered impossible.

The precipitation threshold is reached even at pH = 7.45, equivalent to Ω = 9 (Table 3). However, no precipitation was detected at pH = 7.17 when Ω = 5. It is possible that after a longer stabilization time, the precipitation will appear experimentally. Thus, these results can explain the reason for scaling in natural water circuits despite the low supersaturation coefficients achieved and the prediction made by the MLSI calculation. The thermodynamic predictions must, therefore, be considered with great care before applying any other suggestion.

Table 3 shows the values of different scaling indices calculated at the pH_{stab}. These indices are crucial for determining the potential of calcium carbonate precipitation and scaling in the tested solutions. For the test carried out with an open cell, the calculated values of the three saturation indices prove that calcium carbonate tends to precipitate, and the solution is scale-forming at the threshold pH: LSI > 0, RSI < 6, and MLSI > 0. These results align with the expectation that, under these conditions, calcium carbonate precipitation and scale formation are likely. However, in the case of tests carried out by closing the cell and for a pH_{stab} < 7.8, the two saturation indices, LSI and RSI, show that the solutions are scaling (LSI > 0 and RSI < 6). Contrary to expectation, MLSI < 0 suggests that the solutions are non-scale-forming. This discrepancy indicates that MLSI, which incorporates additional factors beyond pH and calcium concentration, does not align with the expectations based on LSI and RSI. It suggests that despite conditions indicating potential scale formation based on LSI and RSI, MLSI does not support this conclusion, indicating a non-scale formation.

5. Conclusions

Scaling indices are practical tools that have been used to predict scale-forming in water systems for a long time. Theoretical calculations on predefined water solutions show contradictions in results in predicting if water is scale-forming. According to LSI, water scales once the pH exceeds the pH_{eq} of calcite. This same approach was adopted in the MLSI, but with consideration of a metastable zone located between the pHeq of calcite and the monohydrate form of calcium carbonate. Nevertheless, for the Ryznar stability index (RSI), the metastable zone is $CaCO_3$ concentration-dependent. The field study shows that the scale formed in the water distribution systems is mainly calcite ($CaCO_3$), and the main factor in this scale formation is CO_2 degassing. It was shown that RSI is the most suitable for predicting scale formation.

At the laboratory scale, the role of CO_2 degassing rate was underlined. In addition, the reaction time at a given saturation state is a crucial parameter. The nucleation time is widely influenced by the thermodynamic state of the calco–carbonic system. The scaling indices calculation shows, once again, that the RSI is the most adaptable index for predicting if water is scale-forming. This also explains the scaling phenomenon appearing at the industrial scale, where precipitation occurs at low supersaturation coefficients and incrusting on the walls of pipes, reservoirs, pumps, etc.

Author Contributions: Conceptualization, R.H. and M.M.T.; methodology, R.H. and M.M.T.; software, R.H.; validation, R.H. and M.M.T.; formal analysis, R.H. and M.M.T.; investigation, R.H.; resources, R.H. and M.M.T.; data curation, R.H.; writing—original draft preparation, R.H.; writing—review and editing, R.H. and M.M.T.; visualization, R.H.; supervision, R.H. and M.M.T.; project administration, R.H. and M.M.T.; funding acquisition, R.H. and M.M.T. All authors have read and agreed to the published version of the manuscript.

Funding: This research was funded by Prince Sattam bin Abdulaziz University, project number PSAU/2023/01/26520.

Data Availability Statement: Data are available upon reasonable request.

Acknowledgments: The authors extend their appreciation to Prince Sattam bin Abdulaziz University for funding this research work through the project number (PSAU/2023/01/26520).

Conflicts of Interest: The authors declare no conflicts of interest.

References

1. Chhim, N.; Haddad, E.; Neveux, T.; Bouteleux, C.; Teychené, S.; Biscans, B. Performance of green antiscalants and their mixtures in controlled calcium carbonate precipitation conditions reproducing industrial cooling circuits. *Water Res.* **2020**, *186*, 116334. [CrossRef] [PubMed]
2. Kum, S.; Tang, X.; Liu, H. Treatment of brackish water inland desalination brine via antiscalant removal using persulfate photolysis. *Environ. Sci. Water Res. Technol.* **2023**, *9*, 1137–1146. [CrossRef]
3. Chang, B.; Li, G.; Guo, F.; Lu, S.; Peng, Y.; Hou, J. Research on Carbon Dioxide-Assisted Electrocoagulation Technology for Treatment of Divalent Cations in Water. *Water* **2024**, *16*, 1715. [CrossRef]
4. Gebauer, D.; Völkel, A.; Cölfen, H. Stable prenucleation calcium carbonate clusters. *Science* **2008**, *322*, 1819–1822. [CrossRef] [PubMed]
5. Pouget, E.M.; Bomans, P.H.H.; Goos, J.A.C.M.; Frederik, P.M.; de With, G.; Sommerdijk, N.A.J.M. The Initial Stages of Template-Controlled $CaCO_3$ Formation Revealed by Cryo-TEM. *Science* **2009**, *323*, 1455–1458. [CrossRef] [PubMed]
6. Hamdi, R.; Tlili, M.M. Influence of foreign salts on the $CaCO_3$ pre-nucleation stage: Application of the conductometric method. *CrystEngComm* **2022**, *24*, 3256–3267. [CrossRef]
7. Hamdi, R.; Tlili, M.M. Conductometric study of calcium carbonate prenucleation stage: Underlining the role of $CaCO_3{}^o$ ion pairs. *Cryst. Res. Technol.* **2016**, *51*, 99–109. [CrossRef]
8. Mazziotti di Celso, G.; Prisciandaro, M.; Karatza, D.; Musmarra, D.; Lancia, A. Study of the Effect of Leucine on Calcium Carbonate Precipitation in a Circular Economy Perspective. *Water* **2022**, *14*, 270. [CrossRef]
9. Hamdi, R.; Tlili, M.M. Influence of Foreign Salts and Antiscalants on Calcium Carbonate Crystallization. *Crystals* **2023**, *13*, 516. [CrossRef]
10. Al-Hashim, M.H.; Al-Aidaros, A.; Zaidi, F.K. Geological and Hydrochemical Processes Driving Karst Development in Southeastern Riyadh, Central Saudi Arabia. *Water* **2024**, *16*, 1937. [CrossRef]
11. Eichinger, S.; Boch, R.; Leis, A.; Koraimann, G.; Grengg, C.; Domberger, G.; Nachtnebel, M.; Schwab, C.; Dietzel, M. Scale deposits in tunnel drainage systems—A study on fabrics and formation mechanisms. *Sci. Total Environ.* **2020**, *718*, 137140. [CrossRef] [PubMed]
12. Atkinson, G.; Mecik, M. The chemistry of scale prediction. *J. Pet. Sci. Eng.* **1997**, *17*, 113–121. [CrossRef]
13. Zhang, F.; Dai, Z.; Zhang, Z.; Al-Saiari, H.; Yan, F.; Bhandari, N.; Ruan, G.; Liu, Y.; Lu, Y.-T.; Deng, G.; et al. Scaling Risk and Inhibition Prediction of Carbonate Scale at High Temperature. In Proceedings of the SPE International Conference on Oilfield Chemistry, Montgomery, TX, USA, 3–5 April 2017.
14. Coto, B.; Martos, C.; Peña, J.L.; Rodríguez, R.; Pastor, G. Effects in the solubility of $CaCO_3$: Experimental study and model description. *Fluid Phase Equilibria* **2012**, *324*, 1–7. [CrossRef]
15. Grimes, C.J.; Hardcastle, T.; Manga, M.S.; Mahmud, T.; York, D.W. Calcium Carbonate Particle Formation through Precipitation in a Stagnant Bubble and a Bubble Column Reactor. *Cryst. Growth Des.* **2020**, *20*, 5572–5582. [CrossRef]
16. Cosmo, R.d.P.; Ressel Pereira, F.d.A.; Ribeiro, D.d.C.; Barros, W.Q.; Martins, A.L. Estimating CO_2 degassing effect on $CaCO_3$ precipitation under oil well conditions. *J. Pet. Sci. Eng.* **2019**, *181*, 106207. [CrossRef]
17. Cosmo, R.d.P.; Pereira, F.d.A.R.; Soares, E.J.; Ferreira, E.G. Addressing the root cause of calcite precipitation that leads to energy loss in geothermal systems. *Geothermics* **2022**, *98*, 102272. [CrossRef]
18. Cosmo, R.d.P.; Rinaldi, R.; Pereira, F.d.A.R.; Soares, E.J.; Martins, A.L. CO_2 degassing in $CaCO_3$ precipitation in the presence of oil: Implications, modeling, numerical simulation, validation, prototype development, and experimental results. *Geoenergy Sci. Eng.* **2023**, *228*, 211885. [CrossRef]
19. Davies, C.W. *Ion Association*; Butterworths: London, UK, 1962.
20. Malmberg, C.G.; Maryott, A.A. Dielectric constant of water from 0° to 100°C. *J. Res. Natl. Inst. Stand. Technol.* **1956**, *56*, 1–8. [CrossRef]

21. Plummer, L.N.; Busenberg, E. The solubilities of calcite, aragonite and vaterite in CO_2-H_2O solutions between 0 and 90°C, and an evaluation of the aqueous model for the system $CaCO_3$-CO_2-H_2O. *Geochim. Cosmochim. Acta* **1982**, *46*, 1011–1040. [CrossRef]
22. Langelier, W.F. The analytical control of anti-corrosion water treatment. *J. Am. Water Work. Assoc.* **1936**, *28*, 1500–1521. [CrossRef]
23. Ryznar, J.W. A new index for determining amount of calcium carbonate scale formed by a water. *J.-Am. Water Work. Assoc.* **1944**, *36*, 140–153. [CrossRef]
24. Larson, T.E.; Buswell, A.M. Calcium Carbonate Saturation Index and Alkalinity Interpretations. *J. AWWA* **1942**, *34*, 1667–1678. [CrossRef]
25. Gal, J.Y.; Bollinger, J.C.; Tolosa, H.; Gache, N. Calcium carbonate solubility: A reappraisal of scale formation and inhibition. *Talanta* **1996**, *43*, 1497–1509. [CrossRef] [PubMed]
26. Elfil, H.; Roques, H. Prediction of the limit of the metastable zone in the "$CaCO_3$-CO_2-H_2O" system. *AIChE J.* **2004**, *50*, 1908–1916. [CrossRef]
27. Elfil, H.; Hannachi, A. Reconsidering water scaling tendency assessment. *AIChE J.* **2006**, *52*, 3583–3591. [CrossRef]
28. Tlili, M.M. Etude des mécanismes de précipitation de carbonate de calcium. Application à l'entartrage. Phi Thesis, University of Paris, Paris, France, 2002.
29. Manzola, A.S. Contribution à l'étude de la prévention de l'entartrage par les eaux géothermales du sud Tunisien. Ph.D. Thesis, Faculté des Sciences de Tunis, Tunis, Tunisia, 2003.
30. Nefzi, M. Contribution à l'étude de la prévention de l'entartrage des eaux potables : Moyens chimiques et physiques—Étude de cas. Ph.D. Thesis, Faculté des Sciences de Tunis, Tunis, Tunisia, 2004.
31. Gal, J.-Y.; Fovet, Y.; Gache, N. Mechanisms of scale formation and carbon dioxide partial pressure influence. Part II. Application in the study of mineral waters of reference. *Water Res.* **2002**, *36*, 764–773. [CrossRef]
32. Hamdi, R.; Khawari, M.; Hui, F.; Tlili, M. Thermodynamic and kinetic study of $CaCO_3$ precipitation threshold. *Desalination Water Treat.* **2016**, *57*, 6001–6006. [CrossRef]
33. Gache, N. Rôle des formes hydratées du carbonate de calcium dans la rupture de l'état métastable des solutions sursaturées. Ph.D. Thesis, Université Montpellier II, Montpellier, France, 1998.

Disclaimer/Publisher's Note: The statements, opinions and data contained in all publications are solely those of the individual author(s) and contributor(s) and not of MDPI and/or the editor(s). MDPI and/or the editor(s) disclaim responsibility for any injury to people or property resulting from any ideas, methods, instructions or products referred to in the content.